Spatial and Valence Matched Neutralizing DNA-Nanostructure Blocks Wild-Type SARS-CoV-2 and Omicron Variant Infection

Shuang Wan,[+a] Siwen Liu,[+c] Miao Sun,[a] Jialu Zhang,[a] [b] Xinyu Wei,[a] Ting Song,[a] Yuhao Li,[a] Xinyang Liu,[a] Honglin Chen,*[c] Chaoyong Yang,*[a] [b] Yanling Song*[a]

[a] Shuang Wan, , Shuang Wan, Miao Sun, Jialu Zhang, Xinyu Wei, Ting Song, Yuhao Li, Xinyang Liu, Prof. Chaoyong Yang, Prof. Yanling Song
The MOE Key Laboratory of Spectrochemical Analysis & Instrumentation, the Key Laboratory of Chemical Biology of Fujian Province, State Key Laboratory of Physical Chemistry of Solid Surfaces, Department of Chemical Biology, College of Chemistry and Chemical Engineering, Xiamen University
Xiamen, Fujian 361005, China
E-mail: cyyang@xmu.edu.cn; ylsong@xmu.edu.cn.

[b] Prof. Chaoyong Yang
Institute of Molecular Medicine, Renji Hospital, Shanghai Jiao Tong University School of Medicine
Shanghai Jiao Tong University
Shanghai, 200127, China

[c] Dr. Siwen Liu, Prof. Honglin Chen
State Key Laboratory for Emerging Infectious Diseases and InnoHK Centre for Infectious Diseases, Department of Microbiology, Li Ka Shing Faculty of Medicine, the University of Hong Kong, Hong Kong SAR, China.
E-mail: hlchen@hku.hk.

[+] These authors contributed equally to this work.

Supporting information for this article is given via a link at the end of the document.

Abstract: Natural ligand-receptor interactions that play pivotal roles in biological events are ideal models for design and assembly of artificial recognition molecules. Herein, aiming at the structural characteristics of the spike trimer and infection mechanism of SARS-CoV-2, we have designed a DNA framework-guided spatial patterned neutralizing aptamer trimer for SARS-CoV-2 neutralization. The ~5.8 nm tetrahedral DNA framework affords precise spatial organization and matched valence as four neutralizing aptamers (MATCH-4), which matches with nanometer precision the topmost surface of SARS-CoV-2 spike trimer, enhancing the interaction between MATCH-4 and spike trimer. Moreover, the DNA framework provides a dimensionally complementary nanoscale barrier to prevent the spike trimer-ACE2 interaction and the conformational transition, thereby inhibiting SARS-CoV-2-host cell fusion and infection. As a result, the spatial and valence-matched MATCH-4 ensures improved binding affinity and neutralizing activity against SARS-CoV-2 and its varied mutant strains, particularly current Omicron variant that are evasive of the majority of existing neutralizing antibodies. In addition, because neutralizing aptamers specific to other targets can be evolved and assembled, the present design has the potential to inhibit other wide-range and emerging pathogens.

Introduction

The outbreak of SARS-CoV-2 and its variants has underscored the need to rapidly generate specific recognition and treatment strategies against novel pathogens.[1] SARS-CoV-2 presents the unique conformational pattern and transition of the spike trimer, which allow SARS-CoV-2 to bind strongly to host receptor ACE2 via the receptor-binding domain (RBD) on spike protein. Specifically, in uninfected cells, the majority of the spike trimers are in a tightly closed state, and only a minority is in the intrinsically transient open state with one up RBD representing a fusion-prone state. Once the up RBD is trapped by host ACE2, the associated ACE2-RBD complex swings continuously on the topmost surface of the spike trimer to release the constraints imposed on the fusion machinery, thereby promoting virus-cell membrane fusion and viral infection.[2] Therefore, a neutralization strategy that effectively binds to all three RBDs on the spike trimer will block the ACE2-RBD interaction and subsequent conformational transition, thus achieving an ideal therapeutic effect for COVID-19. [3]

Precise and efficient natural recognition is often based on the formation of a complementary pair with series non-covalent bonds and the achievement of the proper interfacial contact. For example, homo-trimeric tumor necrosis factor recruits three tumor necrosis factor receptors to form a complex for immune responses and inflammation.[4] Inspired by the spatial distribution and valence-matched multivalent ligand-receptor interaction, we engineered a multivalent aptamer trough a tetrahedron-conformational DNA holder (MATCH), to achieve a neutralizing reagent trimer for efficient blocking of SARS-CoV-2 infection via binding to three RBDs of the spike trimer.

Neutralizing antibodies show great potential for direct-acting and immediate therapy. [5] However, exact matching of the three-dimensional structure of spike-trimer is difficult to achieve without major costs in yield and quality.[6] In contrast, single-stranded nucleic acids to neutralize SARS-CoV-2, also known as neutralizing aptamers, offer a parallel strategy to rapidly produce potent antiviral reagents for passive immunization.[7] Watson-Crick base pairing results in straight-forward programmability of neutralizing aptamers, thus allowing aptamer-target interaction in a quantitative manner by specific shape and precise valence assembly.[8] In addition, aptamers have favorable chemical and biological properties, including small size, high thermostability, low immunogenicity and deep tissue penetration.[9] Therefore, aptamers have unique advantages over neutralizing antibodies in several aspects and can be engineered as a topologically matched neutralizing reagent for SARS-CoV-2 via DNA nanotechnology. [10]

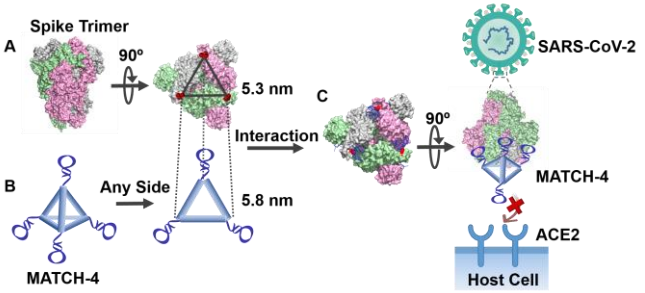

Scheme 1. The mechanism of MATCH strategy for SARS-CoV-2 neutralization. (A) Diagram of trimetric spike protein (PDB code 7KDJ). The three RBDs are depicted in grey, pink, and green, respectively. The representative amino acid residues involved ACE2 binding are indicated in red. (B) A tetrahedral DNA framework based on four neutralizing aptamers (MATCH-4). (C) The mechanism of SARS-CoV-2 neutralization by MATCH-4.

Given that the RBD-RBD distance is ~5 nm on the topmost surface of the spike trimer resembling as an equilateral triangle (Scheme 1A), we strategically designed the MATCH architecture as multivalently arranged neutralizing aptamers in a 2D pattern complementary to an equilateral triangle conformation of the spike trimer (Scheme 1B). Specifically, a ~5.8 nm tetrahedral DNA framework was used as the scaffold to orthogonally anchor aptamers targeting RBDs of the spike trimer. The resultant designs are called MATCH 1-4 with precise spatial organization and quantitative aptamer number. Each side of MATCH-4 has three pieces of neutralizing aptamer arranged in the shape of a ~5.8 nm equilateral triangle (Scheme 1C). Compared to a monomeric aptamer, MATCH-4 with well-matched structure enables spatially patterned multivalent interaction capable of binding three RBDs of spike trimer by three neutralizing aptamers. Moreover, the DNA framework of MATCH-4 also provides a dimensionally complementary nanoscale barrier to prevent the interaction of spike trimer-ACE2 receptor and the conformational transition of the spike trimer, thus further inhibiting SARS-CoV-2-host cell fusion and infection. With the dual blocking MATCH strategy of spatially patterned multivalent aptamer binding and steric hindrance of DNA nanostructure, MATCH-4 is expected to inhibit SARS-CoV-2 infection with high efficiency and to serve as a model for the development of new neutralization mechanisms for possible future pandemics.

Results and Discussion

Characterization of MATCH-n. To construct MATCH assemblies with a series of valence states, we orthogonally anchored the neutralizing aptamers on the tetrahedral DNA framework according to the quantitative ratio to generate MATCH 1-4. The successful assembly of MATCH 1-4 was confirmed by polyacrylamide gel electrophoresis (PAGE) (> 75% yield, Figure 1A&S1). To further analyze the stoichiometry of MATCH 1-4, we characterized the valence of MATCH 1-4 containing gold-nanoparticle modified aptamers by transmission electron microscopy (TEM). As shown in Figure 1B, the number of gold-nanoparticles attached to aptamers extending from the framework is controllable, indicating the successful quantitative construction of MATCH 1-4. Additionally, cryo-electron microscopy images showed the morphology and size of MATCH-4 (Figure 1C), further confirming the formation of the tetrahedral DNA structure.

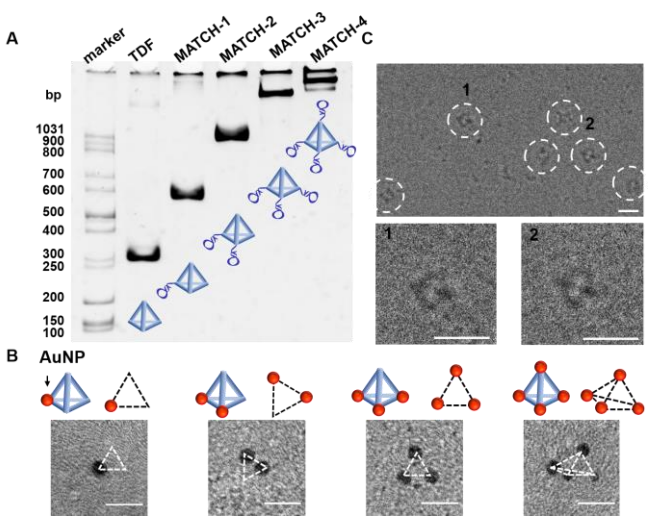

Figure 1. Characterization of MATCH-n. (A) PAGE characterization of tetrahedral DNA framework (TDF) and MATCH 1-4. (B) TEM images of the MATCH-n assembled with quantitative AuNPs (5 nm). Scale bar: 20 nm. (C) The topological structure characterization of MATCH-4 by cryo-electron microscopy. Scale bar: 20 nm.

Binding of MATCH-n against SARS-CoV-2 Spike Trimer. Changes in valence affect the interaction of MATCH-n assembly and SARS-CoV-2 spike trimer (Figure 2A), which will lead to different inhibition effects on virus infection. The K_d (dissociation constant) values of MATCH 1-4 against SARS-CoV-2 spike trimer vary inversely with the number of aptamers at vertices. MATCH-4 shows the smallest K_d value of ~2.4 nM (Figure 2B), which is ~8.2-fold lower than that of MATCH-1, indicating significantly improved binding affinity. With the inability to form multivalent binding, MATCH-1 (or free RBD aptamer) will easily dissociate from the RBD, so it is difficult to bind to three RBDs within one spike trimer at the same time. In contrast, with their well-matched valence and topological structures, MATCH-3 and MATCH-4 exhibit significantly improved binding affinities probably due to the active prompted-aptamer-RBD binding events in the presence of an aptamer bound to an RBD monomer, making it more likely that all three RBDs are bound by three aptamers assembled on MATCH-3 or MATCH-4.

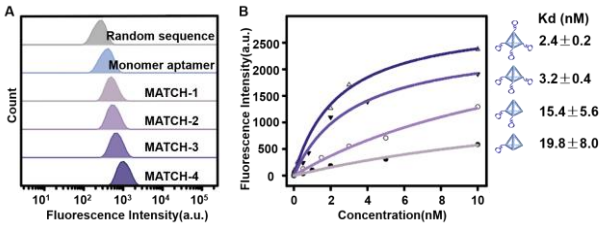

Figure 2. (A) Flow cytometry analysis of the binding of MATCH-n with spike-trimer of SARS-CoV-2. (B) Binding curves and dissociation constants of MATCH-n against spike-trimer of SARS-CoV-2.

Molecular Docking and Molecular Dynamics Simulations. To further understand the mechanism of the valence and topological matching interaction, we performed molecular docking and molecular dynamics simulations (MDS) to study the detailed interactions of MATCH-n and spike-trimer (Figure S2). Considering the computational complexity, the 3D-structures of MATCH 1-4 were simplified as a 5.8 nm equilateral triangle with 1-3 aptamers at the vertices: 1-aptamer for MATCH-1, 2-aptamer for MATCH-2, 3-aptamer for MATCH-3 and MATCH-4. Consistent with the K_d values, the absolute values of the simulated binding free energy change for the n-aptamer and spike trimer increased with the increase of

the number of assembled aptamers. Interestingly, the 3-aptamer and spike trimer complex displayed an approximately 4-fold (not 3-fold) negative binding free energy change (-271 Kcal/mol), compared to that of the 1-aptamer and spike trimer complex (-67 Kcal/mol). The enhancement of binding energy above the multiple of valence states indicates that the clustered aptamer-spike binding is not a simple sum of the several individual aptamer-spike bindings, but that there is a synergistic effect for each individual aptamer-spike binding. As shown in Figure 3, compared to 1-aptamer-binding, 3-aptamer showed not only three binding events, but also that the number of bases involved and the absolute value of the overall binding energy increased (Figure 3). Based on the experimental and simulation results, MATCH-4 has the best binding affinity against spike trimer; so MATCH-4 was chosen for antivirus infection.

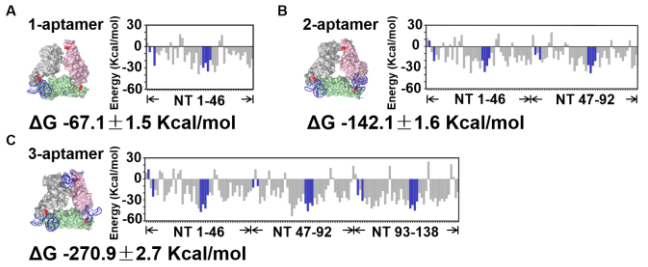

Figure 3. The results of molecular dynamics simulations of (a) 1-aptamer (b) 2-aptamer (c) 3-aptamer. Histogram plot showing the interaction energy between 1-,2-,3-aptamer nucleotide (NT) and spike-trimer. The blue nucleotides were predicted to inhibit RBD-ACE2 interaction.

MATCH-4 Prevention of SARS-CoV-2 Pseudovirus from Entering HEK-293T-ACE2 Cells. To validate the interaction between MATCH-4 and SARS-CoV-2, a pseudotyped lentiviral packaged with the spike trimer gene of SARS-CoV-2 was chosen as SARS-CoV-2 pseudovirus. Cryo-electron microscopy (Cryo-EM) imaging was carried out to directly show the interaction between MATCH-4 and the SARS-CoV-2 pseudovirus. As shown in Figure 4A, MATCH-4 looks like a nanoscale “hat” which wraps over the spike trimer of the pseudovirus. Thus MATCH-4 both enables topologically programmed multivalent aptamer binding, and also provides appropriate steric hindrance of DNA framework to further block the spike-trimer and ACE2 interaction.

Time-lapsed, live confocal imaging was further applied to demonstrate that MATCH-4 prevents SARS-CoV-2 pseudovirus from entering the host cells.[11] The pseudovirus was labeled with DiD (red), and MATCH-4 was labeled with Alex 488 fluorophore (green). When the red pseudovirus and green MATCH-4 co-localized, the merged signals appeared yellow. The finer details between labeled MATCH-4 can be resolved when viewing the separate fluorescence channels (Figure S3). Pseudovirus either pretreated with MATCH-4 or untreated was introduced to pre-stained ACE2-expressing HEK-293T cells. In the untreated situation, the accumulated pseudovirus bonded and entered the host cells over time. In the cells pretreated with MATCH-4, pseudovirus accumulation was drastically reduced, and, even if some pseudoviruses reached the host cell, no obvious virus signal was observed from the cells over more 1.5 hours. Overall, these results established that MATCH-4 can bind to SARS-CoV-2 pseudovirus and prevent SARS-CoV-2 pseudovirus from infecting host cells.

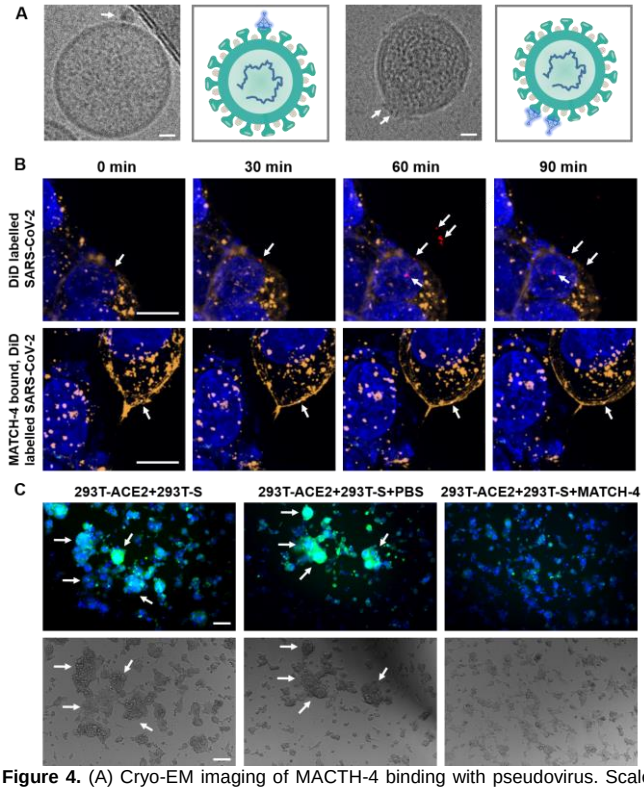

Figure 4. (A) Cryo-EM imaging of MACTH-4 binding with pseudovirus. Scale bar: 20 μm. (B) Time-laped, live confocal imaging. Top row: pseudovirus accumulated to enter the host cells without treatment with unblocking agent. Bottom row: MATCH-4 pre-block pseudovirus entering cells. Scale bar: 20 μm. (C) MATCH-4 block ACE2-293T and Spike-293T cell fusion. ACE2-293T were dyed with Hoechst and Spike-293T were transfected with GFP. Scale bar: 200 μm.

MATCH-4 Inhibition of 293T-ACE2 and 293T-Spike Cell-Cell Fusion. In addition to the interaction of spike trimer and ACE2, the conformational transition of trimeric-spike from a closed state to an open state is another crucial step associated with infection.[12] Since MATCH-4 provides three spatially matched aptamers that can occupy three RBDs on spike trimer, and the DNA framework will further restrict the swing motions of spike trimer, MATCH-4 may inhibit SARS-CoV-2 fusion with the target cells. To investigate this, we used a SARS-CoV-2 spike-mediated cell-cell fusion assay, which is widely used to study virus and targeted cell fusion.[12] 293T cells that can stably express SARS-CoV-2 spike protein (293T-S) and GFP was used as the effector cells while 293T cells that express ACE2 (293T-ACE2) was chosen as the target cells. After 293T-S and 293T-ACE2 cells were co-cultured for 24 h with or without MATCH-4 treatment, the number of 293T-S cells fused with 293T-ACE2 cells was counted. Compared to the group without MATCH-4 treatment, the fusion between 293T-S and 293T-ACE2 cells was significantly blocked by MATCH-4 (Figure 4C). In detail, the groups of untreated and PBS treated 293T-S cells could fuse with 293T-ACE2 cells to form large syncytia which could be easily observed by merging fluorescent images, while a smaller and less syncytium was shown when 293T-S were co-cultured with 293T-ACE2 cells in the presence of MATCH-4. This result indicates that MATCH-4 inhibits 293T-ACE2 and 293T-S cell-cell fusion, leading to reducing of spike trimer-ACE2 complex formation and the subsequent conformational transition of spike trimer.

Pseudotyped SARS-CoV-2 Neutralization. We then evaluated the inhibition ability of MATCH-4 by the pseudovirus neutralization

assay. The SARS-CoV-2 pseudovirus RNA genome contains luciferase and GFP gene. Thus, virus-mediated infection can be determined via intracellular GFP or bioluminescence intensity. Briefly, the SARS-CoV-2 pseudovirus was incubated with different inhibitors and the percentage of remaining infected cells was evaluated by GFP imaging.

The average inhibition efficiencies of MATCH-3 and MATCH-4 at 5 nM were ~82% and ~88%, respectively, both similar to a commercial neuralization antibody (87%, Research Resource Identifiers Number: AB_2857935) at the same dose (Figure 5A-B). In correlation with the K_d results, the MATCH-1 and MATCH-2 provided a relatively lower inhibitory effect, with inhibition efficiency of ~74.3% and ~79.1%, respectively. It's noteworthy that the monomer aptamer exhibits much poorer inhibition (~22.2%) than MATCH-1. Simialry, the inhibition efficiency of MATCH-2 is obviously better than that of the previous circularly bivalent aptamer [7a] at the same concentration (Figure 5A & Figure S4), even though they have the same valence state. This respectively substantial boosts suggest that the nanostructured steric hindrance of DNA framework, as well as spatial and valence matched interaction of the aptamer-spike, both of which can significantly help with antiviral infection. Moreover, MATCH-4 exhibited a high inhibitory activity with a half-maximal inhibitory concentration (IC_{50}) of 0.15 nM (Figure 5C), which is about several times smaller than that of several reported neutralization antibodies and the circularly bivalent aptamer.[7] In addition, the selectivity of MATCH-4 was investigated. Similar to the reported monomer aptamer, MATCH-4 recognizes the spike protein of SARS-CoV-2, but does not bind to RBD/Spike or the key proteins of Mers, HKU and HIV pseudotyped viruses (Figure 5D).

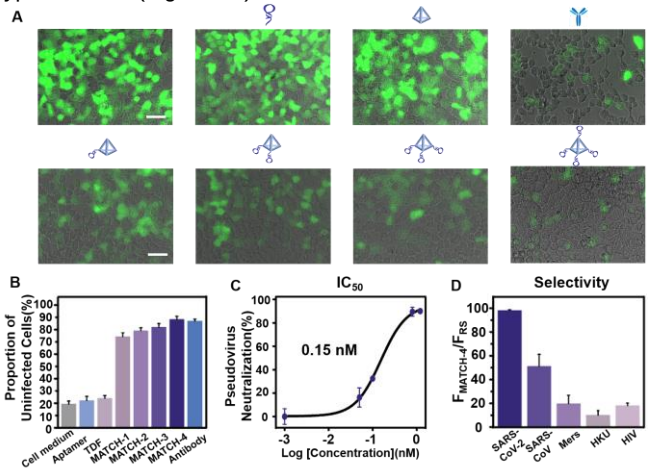

Figure 5. Pseudovirus inhibition by MATCH-n. (A) Fluorescence images and (B) statistical results of cell medium, monomer aptamer, TDN, MATCH-n and neutralization antibody inhibitions of SARS-CoV-2 pseudovirus infection ACE2-expressing HEK-293T. The concentration of these neutralizing reagents was 5 nM. Scale bar: 50 μm. (C) IC_{50} curve assessed by MATCH-4 blocking pseudovirus SARS-CoV-2. (D) Selectivity of MATCH-4 against RBD/Spike or key protein of viruses (SARS-CoV-2, SARS-CoV, Mers, HKU, HIV).

Mutated Pseudotyped SARS-CoV-2 Neutralization. Recently, several new SARS-CoV-2 mutated variants have been rapidly spreading around the world, showing higher transmissibility and are less susceptibility to some existing treatments or vaccines.[13] In particular, the SARS-CoV-2 B.1.1.529 variant (Omicron) contained 15 mutation on the RBD, is reported can escape the majority of existing neutralizing antibodies against SARS-CoV-2.[14] Therefore, there is an urgent need to develop versatile strategies that can respond to different mutant strains.

With improved binding affinity and dual blocking mechanism, MATCH-4 is predicted to have a higher mutation-resistant escape ability compared to monovalent aptamer. As hypothesized, MATCH-4 retains both binding capability (Figure S5-7) and > 85% neutralization efficiency against several current prevalent mutant strains, including D614G, K417N: E484K: N501Y, L452R: E484Q: P681R and Omicron mutant pseudovirus (Figure 6). For example, 91% of the multi-site mutant pseudovirus (L452R: E484Q: P681R) that mimics the dominant circulating Delta strain, was blocked by MATCH-4 from infecting host cells, displaying much higher potency than the monomer aptamer and the neutralizing antibody (Figure 6G). For another current epidemic strain, Omicron variant with 15 mutations on the RBD, MATCH-4 achieved nearly 100% neutralization (Figure 6H). Overall, MATCH-4 showed generally good neutralization effect against a variety of mutant strains, with higher inhibition rates than that of the corresponding monomer aptamer and the neutralization antibody.

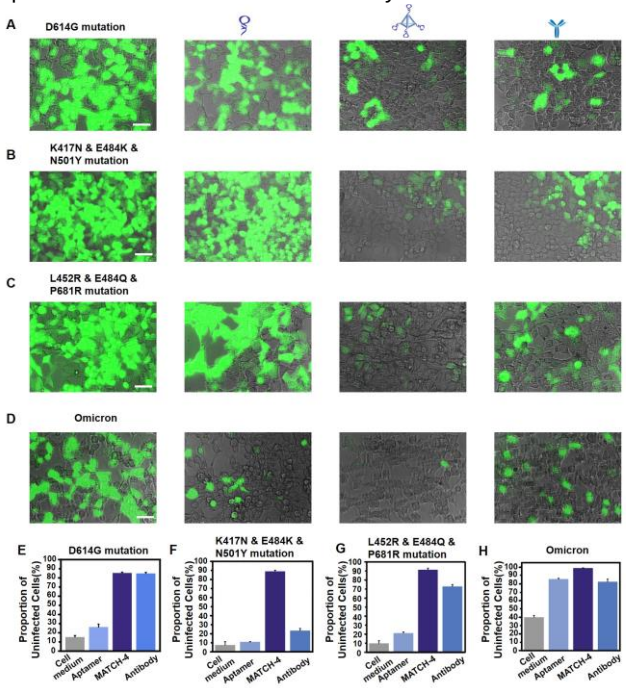

Figure 6. Images of monomer aptamer, MATCH-4 and neutralization antibody block (A) D614G, (B) K417N & E484K & N501Y, (C) L452R & E484Q & P681R and (D) Omicron mutation variant pseudovirus SARS-CoV-2. Average inhibition efficiency against (E) D614G, (F) K417N & E484K & N501Y, (G) L452R & E484Q & P681R and (H) Omicron mutation variant pseudovirus SARS-CoV-2. Scale bar: 50 μm. The concentration of MATCH-4 and the antibody is a quarter of the monomer aptamer.

Authentic SARS-CoV-2 Neutralization. Having demonstrated the enhanced neutralization capacity and suppressed mutational escape of MATCH-4, we tested its inhibitory activity against authentic SARS-CoV-2 with D614G mutation (GenBank: MT835143.1). The infected cells were identified using a comprehensive image analysis, consisting of staining with Alexa Fluor594-conjugated anti-nucleocapsid protein antibody for SARS-CoV-2 virus and Hoechst for DNA content of Vero E6 cell. As shown in Figure 7, more than 85% Vero E6 cells without MATCH-4 treatment were infected, while only about 26% of the cells were infected in the samples treated with MATCH-4. It is noteworthy that most of the viral fluorescent signals with MATCH-4 treatment were on the infected cell membrane, and the intensity and area of viral signal in the cytoplasm were far less than those in the infected cells without MATCH-4 treatment, indicating that, although MATCH-4 could not completely prevent the authentic

SARS-CoV-2 infection, it could still reduce the infection degree of the viruses.

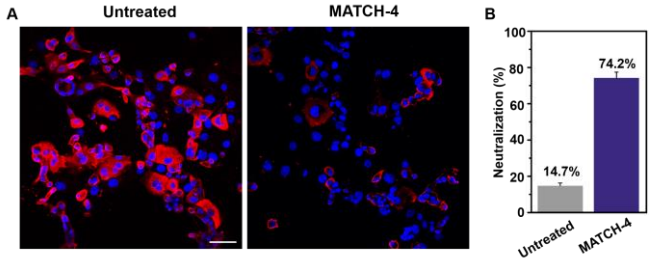

Figure 7. Images of MATCH-4 neutralization of authentic SARS-CoV-2 infection of vero E6 cells and average inhibition efficiency by 1.2 nM MATCH-4. Scale bar: 50 μm.

To further demonstrate the potential of MATCH-4 for the treatment of SARS-CoV-2, the stability and biocompatibility of MATCH-4 were investigated. MATCH-4 is stabe after storage at 4℃ for 15 days and demonstrated a decreased rate of degradation (Figure S8). When testing the safety of MATCH-4, the viability of cells was found unaffected by MATCH-4. More importantly, MATCH-4 did not elicit obvious cell cytotoxicity (Figure S9) nor immune response *in vivo* (Figure S10-11). Furthermore, MATCH-4 did not bind to white blood cells (Figure S12), suggesting no antibody dependent enhancement mediated by Fc fragment.[15] Taken together, the potent inhibition efficiency of MATCH-4 against SARS-CoV-2 through synergetic spatially matched topological multivalent binding and steric hindrance, exhibits excellent stability, biosafety and immunogenicity suggesting that MATCH-4 offers great potential for therapeutics of COVID-19 and other current or emerging coronaviruses.

Conclusion

In conclusion, considering the structural characteristics of spike trimer and the infection mechanism of SARS-CoV-2, we have designed a DNA framework-guided spatially patterned multivalent neutralizing aptamer targeting SARS-CoV-2 neutralization. First, the well-matched topological structure and precise control of the neutralization aptamer organization contribute to significant improvement in binding affinity and neutralization activity. The neutralization effect of MATCH-2 aginat SARS-CoV-2 pseudovirus is better than that of the circularly bivalent aptamer at the same DNA concertation [7a], even each of them contain two aptamers. Moreover, the spatial and valence matched neutralizing aptamer assembly of MATCH-4 avoids the large amounts of wasted disorder aptamers of spherical neutralizing aptamer [10c]. Second, attachment of DNA framework to the RBD-ACE2 binding interface further inhibits SARS-CoV-2 infection because of the steric hindrance from the ~5 nm DNA structure. As a result, compared to the monomer aptamer, the double blocking mechanism of spatially patterned multivalent binding ensures effective neutralizing activity of MATCH-4 against wild type SARS-CoV-2 and its mutant strains, particularly Omicron variant that is evasive of neutralizing antibodies in the current pandemic. In addition, as binders specific to other targets can be evolved and assembled, the present design has the potential to inhibit wide-range and emerging pathogens.

Acknowledgements

We thank the National Natural Science Foundation of China (22022409, 21735004, 21874089), and the Program for Changjiang Scholars and Innovative Research Team in University (IRT13036).

Keywords: DNA nanotechnology • spatial patterned interaction ••neutralizing aptamer • SARS-CoV-2 neutralization • Omicron

[1] C. Wang, P. W. Horby, F. G. Hayden, G. F. Gao, *The Lancet* **2020**, *395*, 470-473.

[2] a) C. Xu, Y. Wang, C. Liu, C. Zhang, W. Han, X. Hong, Y. Wang, Q. Hong, S. Wang, Q. Zhao, Y. Wang, Y. Yang, K. Chen, W. Zheng, L. Kong, F. Wang, Q. Zuo, Z. Huang, Y. Cong, *Sci. Adv.* **2021**, *7*, 5575-5587; b) D. J. Benton, A. G. Wrobel, P. Xu, C. Roustan, S. R. Martin, P. B . Rosenthal, J. J. Skehel, S. J. Gamblin, *Nature* **2020**, *588* , 327-330.

[3] S. Du, Y. Cao, Q. Zhu, P. Yu, F. Qi, G. Wang, X. Du, L. Bao, W. Deng, H. Zhu, J. Liu, J. Nie, Y. Zheng, H. Liang, R. Liu, S. Gong, H. Xu, A. Yisimayi, Q. Lv, B. Wang, R. He, Y. Han, W. Zhao, Y.Bai, Y. Qu, X. Gao, C. Ji, Q. Wang, N. Gao, W. Huang, Y. Wang, X. S. Xie, X.-d. Su; J. Xiao, C. Qin, *Cell* **2020**, *183*, 1013-1023.

[4] J. R. Cochran, D. Aivazian, T. O. Cameron, L. J. Stern, *Trends Biochem. Sci.* **2001**, *26*, 304-310.

[5] Y. Cao, B. Su, X. Guo, W. Sun, Y. Deng, L. Bao, Q. Zhu, X. Zhang, Y. Zheng, C. Geng, X. Chai, R. He, X. Li, Q. Lv, H. Zhu, W. Deng, Y. Xu, Y. Wang, X. S. Xie, *Cell* **2020**, *182*, 73-84 e16.

[6] R. Shi, C. Shan, X. Duan, Z. Chen, P. Liu, J. Song, T. Song, X. Bi, C. Han, L. Wu, G. Gao, X. Hu, Y. Zhang, Z. Tong, W. Huang, W. J. Liu, G. Wu, B. Zhang, L. Wang, J. Qi, H. Feng, F. S. Wang, Q. Wang, G. F. Gao, Z. Yuan, J. Yan, *Nature* **2020**, *584*, 120-124.

[7] a) M.Sun, S. Liu, X. Wei, S. Wan, M. Huang, T. Song, Y. Lu, X. Weng, Z. Lin, H. Chen, Y. Song, C. Yang, *Angew. Chem., Int. Ed.* **2021**, *60*, 10266-10272; b) A. Schmitz, A. Weber, M. Bayin, S. Breuers, V. Fieberg, M. Famulok, G. Mayer, *Angew. Chem., Int. Ed.* **2021**, *60*, 10279-10285; c) X. Liu, Y. L. Wang, J. Wu, J. Qi, Z. Zeng, Q. Wan, Z. Chen, P. Manandhar, V. S. Cavener, N. R. Boyle, X. Fu, E. Salazar, S. V. Kuchipudi, V. Kapur, X. Zhang, M. Umetani, M. Sen, R. C. Willson, S. H. Chen, Y. Zu, *Angew. Chem. Int. Ed.* **2021**, *60*, 10273-10278.

[8] a) L. Wu, Y. Wang, X. Xu, Y. Liu, B. Lin, M. Zhang, J. Zhang, S. Wan, C. Yang, W. Tan, *Chem. Rev.* **2021**, *121*, 12035-12105; b) M. Li, H. Ding, M. Lin, F. Yin, L. Song, X. Mao, F. Li, Z. Ge, L. Wang, X. Zuo, Y. Ma, C. Fan, *J. Am. Chem. Soc.* **2019**, *141*, 18910-18915.

[9] a) S. Zhao, R. Tian, J. Wu, S. Liu, Y. Wang, M. Wen, Y. Shang, Q. Liu, Y. Li, Y. Guo, Z. Wang, T. Wang, Y. Zhao, H. Zhao, H. Cao, Y. Su, J. Sun, Q. Jiang, B. Ding, *Nat. Commun.* **2021**, *12*, 1-10. b) D. Jiang, Z. Ge, H.-J. Im, C. G. England, D. Ni, J. Hou, L. Zhang, C. J. Kutyreff, Y. Yan, Y. Liu, S. Y. Cho, J. W. Engle, J. Shi, P. Huang, C. Fan, H. Yan, W. Cai, *Nat. Biomed. Eng.* **2018**, *2*, 865-877; c) Y. Yang, Q. Lu, C.-M. Huang, H. Qian, Y. Zhang, S. Deshpande, G. Arya, Y. Ke, S. Zauscher, *Angew.Chem. Int. Ed.* **2021**, *60*, 23241-23247; d) Q. Li, L. Liu, D. Mao, Y. Yu, W. Li, X. Zhao, C. Mao, *J. Am. Chem. Soc.* **2020**, *142*, 665-668.

[10] a) E. Benson, A. Mohammed, J. Gardell, S. Masich, E. Czeizler, P. Orponen, B. Hogberg, Nature 2015, 523, 441-449; b) Z. Zhang, R. Pandey, J. Li, J. Gu, D. White, H. D. Stacey, J. C. Ang, C.-J. Steinberg, A. Capretta, C. D. M. Filipe, K. Mossman, C. Balion, M. S. Miller, B. J. Salena, D. Yamamura, L. Soleymani, J. D. Brennan, Y. Li, *Angew.Chem. Int. Ed.* **2021**, *60*, 24266-24274; c) M. Sun, S. Liu, T. Song, F. Chen, J. Zhang, J. Huang, S. Wan, Y. Lu, H. Chen, W. Tan, Y. Song, C. Yang, *J. Am. Chem. Soc.* **2021**, 143, 21541–21548

[11] P. S. Kwon, S. Ren, S. J. Kwon, M. E. Kizer, L. Kuo, M. Xie, D. Zhu, F. Zhou, F. Zhang, D. Kim, K. Fraser, L. D. Kramer, N. C. Seeman,

J. S. Dordick, R. J. Linhardt, J. Chao, X. Wang, *Nat. Chem.* **2020**, *12*, 26-35.

[12] P.-A. Koenig, H. Das,; H. Liu, B. M. Kümmerer, F. N. Gohr, L.- M. Jenster, L. D. J. Schiffelers, Y. M. Tesfamariam, M. Uchima, J. D. Wuerth, K. Gatterdam, N. Ruetalo, M. H. Christensen, C. I. Fandrey, S. Normann, J. M. P. Tödtmann, S. Pritzl, L. Hanke, J. Boos, M. Yuan, X. Zhu, J. L. Schmid-Burgk, H. Kato, M. Schindler, I. A. Wilson, M. Geyer, K. U. Ludwig, B. M. Hällberg, N. C. Wu, F. I. Schmidt, *Science* **2021**, *371*, eabe6230

[13] a) B. Zhou, T. T. N. Thao, D. Hoffmann, A. Taddeo, [13] N. Ebert, F. Labroussaa, A. Pohlmann, J. King, S. Steiner, J. N. Kelly, J. Portmann, N. J. Halwe, L. Ulrich, B. S. Trueb, X. Fan, B. Hoffmann, L. Wang, L. Thomann, X. Lin, H. Stalder, B. Pozzi, S. de Brot, N. Jiang, D. Cui, J. Hossain, M. M. Wilson, M. W. Keller, T. J. Stark, J. R. Barnes, R. Dijkman, J. Jores, C. Benarafa, D. E. Wentworth, V. Thiel, M. Beer, *Nature* **2021**, *592*, 122-127; b) Y. Wang, C. Xu, Y. Wang, Q. Hong, C. Zhang, Z. Li, S. Xu, Q. Zuo, C. Liu, Z. Huang, Y. Cong, *Nat. Commun.* **2021**, *12*, 7345-7357.

[14] Y. Cao, J. Wang, F. Jian, T. Xiao, W. Song, A. Yisimayi, W. Huang, Q. Li, P. Wang, R. An, J. Wang, Y. Wang, X. Niu, S. Yang, H. Liang, H. Sun, T. Li, Y. Yu, Q. Cui, S. Liu, X. Yang, S. Du, Z. Zhang, X. Hao, F. Shao, R. Jin, X. Wang, J. Xiao, Y. Wang, X. Xie, *Nature* **2021**, doi.org/10.1038/d41586-021-03796-6.

[15] W. S. Lee, A. K. Wheatley, S. J. Kent, B. J. DeKosky, *Nat. Microbiol.* **2020**, *5*, 1185-1191.

Entry for the Table of Contents

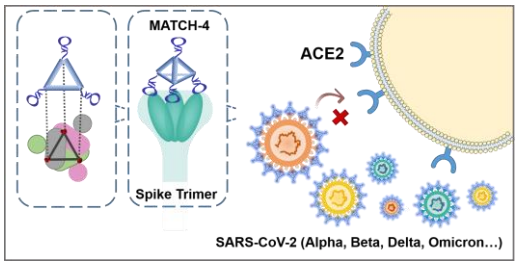

Aiming at the structural characteristics of the spike trimer, we design a DNA framework-guided spatial patterned neutralizing aptamer trimer for SARS-CoV-2 neutralization. With advantages of the spatial and valence matched interaction of aptamer-spike, and dimensionally complementary nanoscale barrier of DNA framework, this strategy can inhibit the infection of SARS-CoV-2 and its varied mutant strains, particularly current Omicron variant.